FRACTOGRAPHY OF WASPALOY WIRE DEPOSITED WITH LASER AND ARC ADDITIVE MANUFACTURING PROCESSES

N.I.S. Hussein[1], M.N. Ayof[1], Y.H.P. Manurung[2], I.R. Pashby[3] and J. Segal[4]

[1]Faculty of Manufacturing Engineering,
Universiti Teknikal Malaysia Melaka, Hang Tuah Jaya, 76100 Durian Tunggal, Melaka, Malaysia.

[2]Faculty of Mechanical Engineering
Universiti Teknologi MARA, 40450 Shah Alam, Selangor, Malaysia.

[3]Peninsula College,
Persiaran Sungai Hampar, 40460 Shah Alam, Selangor, Malaysia.

[4]Faculty of Engineering,
The University of Nottingham, University Park, Nottingham, NG7 2RD, United Kingdom.

Corresponding Author's Email: [1]izan@utem.edu.my

Article History: Received 15 November 2021; Revised 2 April 2022; Accepted 8 June 2022

ABSTRACT: Welding with filler material can be considered as an additive manufacturing process whereby it involves the deposition of molten metal in a form of droplets onto a substrate. Wire and Arc Additive Manufacturing (WAAM) and laser direct metal deposition (DMD) are applied for repair purposes, hard facing, and building structures in various industries such as the aerospace industry. In this research, High-Powered Diode Laser (HPDL) and Gas Tungsten Arc Welding (GTAW) were used as the heat sources to deposit Waspaloy wire layer-by-layer to form a thin wall. The heat flow during the deposition process causes a change in the microstructural and mechanical properties of the subsequent layers. Following the deposition process, solution treatment and aging heat treatment were performed on the Waspaloy thin wall. Understanding the process/property relationship is crucial to ensure the reliability of the built structure. Tensile testing was performed prior to fractography. Fractography is critical to the failure analysis of metals. The objective of this research is to study the microstructure at the fracture surface of wrought Waspaloy, as-deposit, and the heat-treated thin wall, in which it was observed by using a scanning electron microscope (SEM).

Fracture surfaces of samples tested transverse and parallel to the deposition height show major difference. SEM fractography revealed an intergranular failure in the wrought Waspaloy. The laser and arc deposited Waspaloy both show fractures by microvoid coalescence initiated by interdendritic particles. Fractography analysis in this research has effectively employed to identify the fracture origin, failure mechanism, material defects, and the nature of stresses.

KEYWORDS: *Fractography; High-Power Diode Laser; Gas Tungsten Arc Welding; Metal Deposition; Wire and Arc Additive Manufacturing*

1.0 INTRODUCTION

Considering fusion welding with feed material as an additive manufacturing process (AM), it was seen as a suitable process for the layer-by-layer deposition known as various names such as Wire and Arc Additive Manufacturing (WAAM) [1], direct metal deposition (DMD) [2], shape metal deposition (SMD) [3] and metal wire deposition [4]. The three-dimensional (3D) structure is produced by layer-wise AM of thin two-dimensional (2D) cross-sections until a final geometry is acquired. The principle of AM is similar to conventional fusion whereby a heat source is used to melt the substrate and filler material. The filler material is then fused into the melt pool. Metal wire has advantages over powder as a filler material or feedstock for the AM [5]. Apart from its cleanliness when compared to metal powders, the metal wire has higher material usage efficiency and the deposition rate for wire feeding was found to be much higher than powder feeding. Microstructures for both methods were similar, but the surface finish was found to be better for wire-feed samples [6]. Another merit is that metal wires are easily available and cheaper than powder, which makes the wire deposition very cost-competitive [7]. Heat sources used in various types of metal wire AM process include electric arc [1, 3], plasma arc [8], electron beam [9], and laser [4]. In this research, Gas Tungsten Arc Welding (GTAW) and High-powered Diode Laser (HPDL) was used as the heat sources for the AM process.

Waspaloy is a nickel-based superalloy which developed to improve the strength-to-weight ratios at useful service temperatures of up to 954°C of the jet engine [10]. The service temperature is typically up to 650°C for critical rotating parts and closer to 850°C for less demanding static applications [11]. The microstructure of Waspaloy mainly comprises of an austenitic FCC, solid solution, γ-phase matrix, γ'precipitates phase (FCC ordered $Ni_3(Al, Ti)$), and carbide particles [12]. Considering the dynamic changes of microstructural properties that affect the

mechanical properties of Waspaloy following DMD and WAAM processes [10], solution treatment and aging commonly performed to eliminate non-uniform composition. More uniform microstructure and high hardness, as well as high tensile strength of the deposits, can provide suitable material for use in aero engines and other applications [13]. Heat treatment of Waspaloy involves heating to a temperature above the γ′solvus temperature to dissolve the coarse γ′structure, followed by rapid cooling and reheating to a temperature below the γ′solvus for controlled re-precipitation of the γ′phase on a fine-scale [12].

Based on the literature review, it was evident that most of the researchers working on the laser DMD and WAAM processes were interested in the effect of process parameters on the microstructural [7] and mechanical properties such as tensile properties [13] and microhardness [4], metal transfer mode [8] and heat flow modeling [10]. Fractography on the fractured surface of the deposits was found to be still very limited available information. Fractography is critical to the failure analysis of metals. Therefore, the objective of this research is to study the microstructure at the fracture surface of wrought Waspaloy, as-deposit, and the heat-treated thin wall. Fractography analysis in this research was hoped to identify the fracture origin, failure mechanism, material defects, and the nature of stresses.

2.0 METHODOLOGY

Two different deposition systems i.e. HPDL and GTAW were used in this research and both comprised of an energy delivery system, wire feeding apparatus, and CNC for controlling the gantry (in HPDL process) and robot (in GTAW process) movement, and work table motion. These two systems also consisted of an atmosphere control system including argon supply and an oxygen sensor (Dansensor) and a camera system for process control and monitoring. DMD of HPDL was performed with a Rofin Sinar DL025 and the WAAM process was performed with a Hitachi Inverter 500GP3 welding power source with the GTAW torch was attached to the KR15/2 6-axis robot. A 3.2 mm diameter tungsten electrode was grounded to a conical angle of 60°. The GTAW WAAM process was also conducted in a controlled argon atmosphere.

The wire material used in this research was Waspaloy which had a 1.2 mm diameter. Waspaloy walls were deposited onto 10 mm thick Waspaloy substrate. The nominal compositions of the wire and substrate are given in Table 1.

Table 1: Nominal compositions of the Waspaloy wire and substrate (in wt.%)

Material	Element (wt.%)							
	Ni	Cr	Co	Mo	Ti	Al	Fe	C
Wire	Bal.	19.1	13.2	4.3	3.0	1.4	0.9	0.1
Substrate	Bal.	19.8	12.8	4.5	3.1	1.4	0.7	0.1

The optimization of the deposition parameters has been conducted in previous studies [10]. A list of parameters that have proven feasible to produce pore and crack-free deposited structures are listed in Table 2. Heat input per unit length during deposition using DMD of HPDL and WAAM of GTAW was 742 and 400 J/mm, respectively.

Table 2: Parameter for DMD of Waspaloy wire using HPDL and GTAW

Heat Sources									
HPDL	Parameter	Laser Power (kW)	Traverse Speed (m/s)	Wire Feed Rate (m/s)	Step Height (mm)	Work Angle (°)			
	Values	2	0.0017	0.025	2	45			
GTAW	Parameter	Peak Current (A)	Base Current (A)	Voltage (V)	Frequency (Hz)	Traverse Speed (m/s)	Wire Feed Rate (m/s)	Step Height (mm)	Work Angle (°)
	Values	175	95	10.2	8	0.0035	0.015	1	45

Thin walls of dimension ~120 x 120 mm were built as in Figure 1. Fractography was performed after the thin walls were being subjected to tensile testing. Since dimensional changes can occur during aging, finish machining for the tensile testing bar was performed after the heat treatment process. Figure 1 also shows the position of samples were from the thin wall for the heat treatment, tensile testing, and fractography. The thin wall was cut at transverse (T) and perpendicular (P) to the deposition build-up so that fractography and fracture analysis at a different plane of the layer interface could be determined. Heat treatment conditions were solution treatment (ST) and solution treatment and double aging (STA). The ST involved heating up for 20K/min to 1080°. The STA involved the ST conditions, stabilization for 845°C/24 hours/air cooling and aging for 760°C/16 hours/air cooling.

Tensile testing procedure and results were reported in previous studies [*2]. Following the tensile testing, fracture analysis was performed on the fractured samples. The fracture surface was dried with air, put in a sealed plastic bag, and stored in a desiccator. It was necessary to cut 10 mm length from the fracture surface of the fractured tensile test bar for fracture analysis and fractography under the scanning electron microscope (SEM). The fracture surface was cut using a cut-off machine

where the coolant was used. The fracture surface was solvent cleaned and dried immediately in warm air after cutting. Finally, the fracture surface was analyzed under SEM to characterize its type of fracture and to identify the location of the fracture-initiating site.

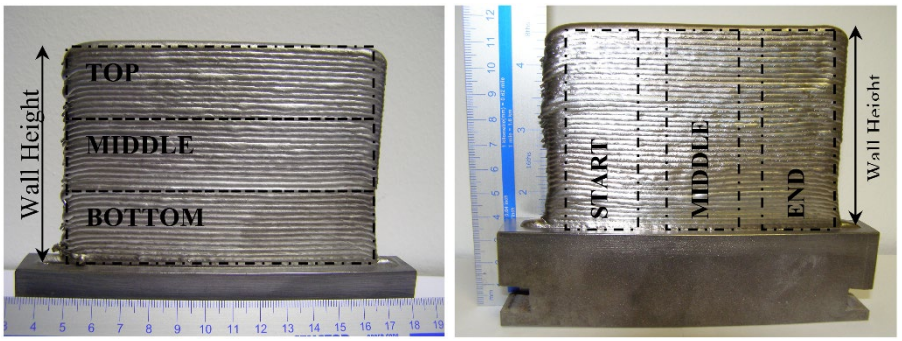

Figure 1: Photograph of the laser deposited Waspaloy thin wall showing (a) the top, middle, and bottom sections transverse (T) to the build direction and (b) the start, middle, and end sections parallel (P) to the build direction.

3.0 RESULTS AND DISCUSSION

Tensile testing was performed on the wrought, as-deposited, and heat-treated Waspaloy. The fractured occurred within the gauge length. The width and thickness of the samples were 6 mm and 3 mm, respectively. Figure 2 shows the macrograph of a cross-section through tensile fracture of (a) ST, (b) STA wrought Waspaloy, (c-h) laser, and (i-n) arc deposited Waspaloy. The macrographs for laser and arc deposited Waspaloy were taken for the middle sections of the thin wall.

3.1 Fractography of Wrought Waspaloy

In the case of wrought Waspaloy, macroscopic fracture surface for the ST material sheared with the fracture inclined at ~45° and for STA material fracture was perpendicular to the tensile axis as shown in Figure 2 (a) and (b), respectively. The overall morphology of the fracture surfaces for W(ST) and W(STA) samples is shown in the SEM fractography, Figure 3, at low and high magnifications. For the W(ST) material fracture occurred along the grain boundaries. Examination of the tensile fractures at the higher magnification indicates that grain boundary cracking and shallow dimpling can be seen. There are dimples of varying sizes with shallow and fine microscopic voids. In the W(STA) sample, similar features are seen but with uniformly distributed and deeper microscopic voids. Grain boundary cracking is also visible. The intergranular dimple rupture in the W(STA) sample is

more substantial than in the W(ST) material. The $M_{23}C_6$ type carbide was detected at the grain boundary of the W(STA) sample. These dimples and microscopic voids from both W(ST) and W(STA) samples indicate they have experienced ductile fracture by microvoid coalescence. Grain boundary cracking is probably initiated around grain boundary carbides.

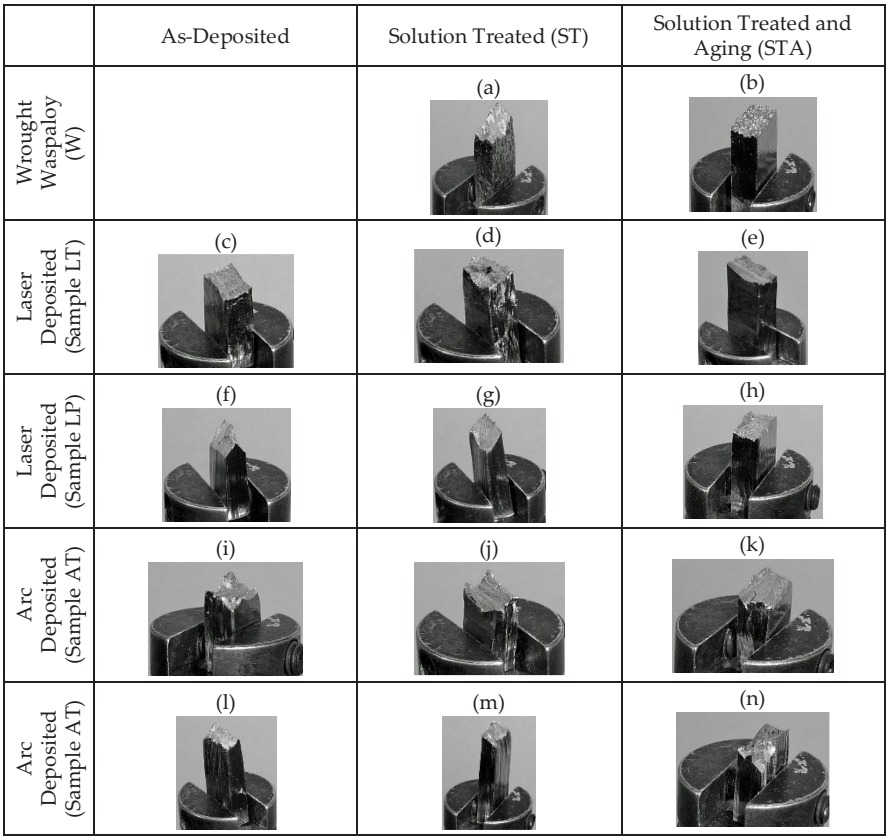

Figure 2: Macrograph of a cross-section through tensile fracture of (a) ST, (b) STA wrought Waspaloy, (c-h) laser, and (i-n) arc deposited Waspaloy.

3.2 Fractography of Laser Deposited Waspaloy

On the macroscopic scale, the tensile fracture of the LT material was by shear with the fracture inclined at ~30° to the tensile axis as shown in Figure 2 (c). The overall morphology of the fracture surfaces for LT samples is shown in Figure 4 (a) and exhibits a clear dendritic pattern with interdendritic cracking. This suggests that the fracture took preferentially along the interdendritic region. The interdendritic cracking probably occurred at the dendrite boundaries and initiated around the interdendritic carbides. There are dimples with fine

microscopic voids indicating a ductile failure by microvoid coalescence. MC type carbide was detected in the microvoids (Figure 4 (b)).

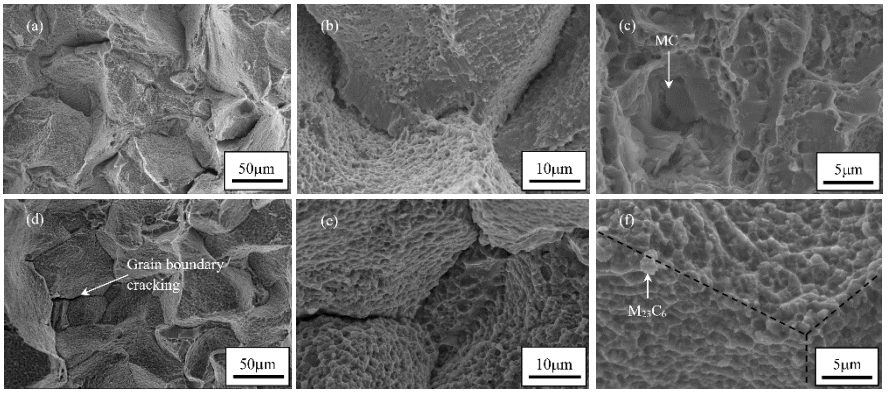

Figure 3: SEM micrographs showing fracture surface features of samples taken from wrought Waspaloy following (a-c) ST, and (d-f) STA.

Tensile fracture of the LP material was by a combination of shear with the fracture surface inclined at ~30° and perpendicular to the tensile stress as displayed in Figure 2 (f). The fracture surfaces of the LP samples as shown in Figure 4 (c) reveal a dendritic pattern with a cruciform shape. Interdendritic cracking was noted. Dimples and microscopic voids observed at higher magnification indicate the sample has experienced ductile fracture by microvoid coalescence. MC type of carbides was found in the dimples suggesting the potential location of fracture initiation. The cruciform pattern is prominent due to the ductile shear of the dendrites, which probably the last feature to have failed during the test.

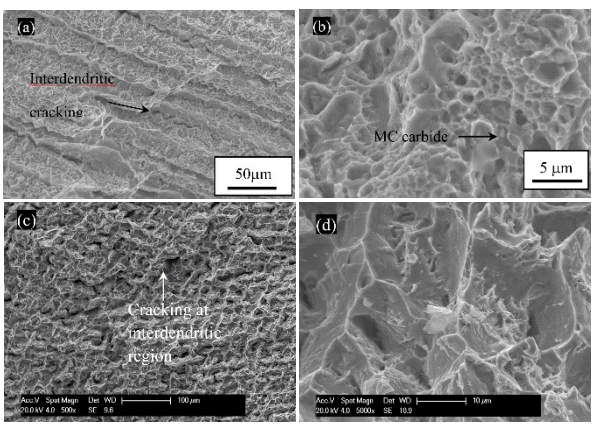

Figure 4: SEM micrographs showing fracture surface features of (a-b) LT, and (c-d) LP material.

3.3 Fractography of Arc Deposited Waspaloy

Tensile fracture of the AT material, which is represented by Figure 2 (i) was almost perpendicular to the tensile axis at the width of the test bar but shear approximately 45° at the thickness of the test bar. The overall morphology of the fracture surfaces for AT samples, as shown in Figure 5, exhibits a clear dendritic pattern similar to the LT materials. However, the dendritic pattern for the AT material appears to be smaller. The fracture surface features of the AT are similar to the LT in regard to the dendritic pattern, interdendritic cracking that might be initiated by the by grain boundary MC type of carbides, and dimples with microscopic voids which indicate a ductile fracture.

On the macroscopic scale, the tensile fracture of the AP material was perpendicular to the tensile stress as in Figure 2 (l). The overall morphology of the fracture surfaces for AP samples as shown in Figure 5 exhibit similar to the LP in regard to the dendritic pattern, interdendritic cracking, and dimples with microscopic voids which indicate a ductile fracture. However, the interdendritic cracking is more apparent in AP than LP materials.

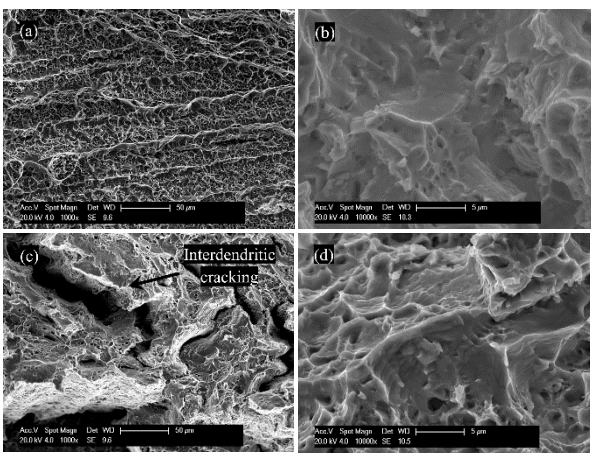

Figure 5: SEM micrographs showing fracture surface features of (a-b) AT, and (c-d) AP material.

3.4 Fractography of Heat-treated Deposited Waspaloy

The tensile fractures of the LT(ST) were by shear with the fracture surface inclined at ~45° to the tensile stress at the thickness of the tensile test bar as shown in Figure 2 (d). Similarly, the fracture surface of AT(ST) samples was also sheared with an inclination of ~45° to the tensile stress (Figure 2 (j)). The overall morphology of the fracture surfaces for LT(ST) and AT(ST) samples exhibits a similar feature

which showing a dendritic pattern although dendrites were significantly reduced after the solution treatment. Interdendritic cracking could be observed in both LT(ST) and AT(ST) materials. The fracture surface feature of the LT(ST) is similar to the AT(ST) in regard to the dendritic pattern, interdendritic cracking by grain boundary MC type of carbides, and dimples with microscopic voids which indicate a ductile fracture.

In the case of LT(STA) and AT(STA), the macroscopic fracture surface was perpendicular to the tensile axis as shown in Figure 2 (e) and (k). The overall morphology of the fracture surfaces for LT(STA) and AT(STA) samples exhibits a similar feature which showing a dendritic 'ghost' pattern. The dendrites were significantly reduced after the solution treatment. The formation of the dendritic pattern in the fracture surface might be due to the carbide phase in the interdendritic region. Interdendritic cracking could be observed in both LT(STA) and AT(STA) materials. Interdendritic cracking by the grain boundary carbides was noted. The $M_{23}C_6$ type of carbides was detected at the fracture surface. Dimples with microscopic voids indicating ductile fracture and particles observed in the dimples are most likely to be the fine γ' precipitates.

On a macroscopic scale, the tensile fractures of the LP(ST) and AP(ST) samples were by shear with the fracture surface inclined at ~45° to the tensile axis as shown in Figure 2 (g) and (m), respectively. The overall morphology of the fracture surfaces for LP(ST) and AP(ST) samples exhibits similar features which showing a dendritic pattern with cruciform shape although dendrites were significantly reduced after the solution treatment. Interdendritic cracking by grain boundary MC type of carbides could be observed in both LP(ST) and AP(ST) materials. Dimples with microscopic voids which indicating ductile fracture was evidently similar.

In the case of LP(STA) and AP(STA), the macroscopic fracture surface was perpendicular to the tensile axis as shown in Figure 2 (h) and (n). The fracture surface feature of the LP(STA) was similar to the AP(STA) in regard to the dendritic 'ghost' pattern and grain boundary cracking. The $M_{23}C_6$ type of carbides was detected at the fracture surface. Dimples with microscopic voids indicating ductile fracture and particles observed in the dimples are most likely to be the fine γ' precipitates. Intergranular fracture in LP(STA) and AP(STA) material was more apparent as compared to those as-deposited and solution treated. This is might due to the formation of a film of M23C6 type of carbides [10].

3.3 Failure Mechanism in Different Samples

Examination of the tensile fracture surfaces does provide useful information pertaining to the effect of microstructural features on the strength and ductility of the samples employed in this research. Fractography of the wrought and directly deposited Waspaloy in their as-deposited condition and following ST and STA showed dimpled fracture surface, which is the characteristic of ductile fracture. Failure in ductile solids arises from the concentration of plastic deformation into a localized region [14]. During straining in the direction of the tensile axis, there exists a tendency for inhomogeneous deformation due to the shearing of the strengthening precipitates dispersed through the alloy matrix. The inhomogeneous deformation is concentrated in certain specific regions of the microstructure and is referred to as being localized [15]. The inhomogeneous deformation is conducive for the formation of an array of macroscopic cracks as was observed for instance in the AT(STA) and AP(STA) materials. In addition, nucleation of microvoids initiated at the second-phase particles undergone considerable growth, and their eventual coalescence results in shallow dimples. Nucleation of microvoids at these particles could begin at the stage as early as after the yield point [14].

As a result of the nature of the ductile fracture, the ductility of the W(STA), AT(STA), AP(STA), LT(STA), and LP(STA) samples significantly decreased with the increase of γ'precipitates. A similar observation was obtained by Zhang [16] who studied the fractography of laser deposited Inconel 718.

Inclusion was observed in the LTT sample, only partial bonding is obtained between this inclusion and the surrounding material and thus, this is also creating porous deposited material. When the pore is under tensile stress, severe stress concentration occurs. Consequently, a crack may occur and become a highly stressed region that propagates further cracking and fracture.

4.0 CONCLUSION

Fracture surfaces of samples tested transverse and parallel to the deposition height show major difference. The tensile strength and ductility could be predicted to be definitely lower when the tensile axis was perpendicular to the growth of the grain which was caused by the crack propagation by the carbide at the grain boundaries. SEM fractography revealed an intergranular failure in the wrought

Waspaloy. The laser and arc deposited Waspaloy both show fractures by microvoid coalescence initiated by interdendritic particles. Fractography analysis in this research has effectively employed to identify the fracture origin, failure mechanism, material defects, and the nature of stresses.

ACKNOWLEDGMENTS

The authors would like to thank the Faculty of Manufacturing Engineering, Universiti Teknikal Malaysia Melaka, and the University of Nottingham, United Kingdom for educational, technical, and financial support through the grant of PJPPC/2020/FKP-COSSID/SC0002.

REFERENCES

[1] A. Ermakova, A. Mehmanparast, S. Ganguly, J. Razavi and F. Berto, "Investigation of mechanical and fracture properties of wire and arc additively manufactured low carbon steel components", *Theoretical and Applied Fracture Mechanics*, vol. 109, pp. 1-9, 2020.

[2] N.I.S. Hussein, M.S.E. Sayuti and M.N. Ayof, "Direct metal deposition of stainless steel wire using metal inert gas as heat source for repair purposes", *Applied Mechanics and Material,* vol. 110-116, pp. 3570-3574, 2011.

[3] A.A. Ugla, H.J. Khaudair, and A.R.J. Almusawi, "Metal inert gas welding-based-shaped metal deposition in additive layered manufacturing: a review", *International Journal of Mechanical and Materials Engineering,* vol. 13, no. 3, pp. 244-257, 2019.

[4] Q. Li, J. Chen, X. Wang, Y. Liu, K. Jiang, S. Yang and Y. Liu, "Process, microstructure and microhardness of GH3039 superalloy processed by laser metal wire deposition", *Journal of Alloys and Compounds*, vol. 877, pp. 1-12, 2021.

[5] B. Blinn, P. Lion, O. Jordan, S. Meiniger, S. Mischliwski, C. Tepper, C. Glabner, J.C. Aurich, M. Weigold and T. Beck, "Process-influenced fatigue behavior of AISI 316L manufactured by powder- and wire-based laser direct energy deposition", *Materials Science and Engineering A,* vol. 818, pp. 1-10, 2021.

[6] S.H. Mok, G. Bi, J. Folkes and I. Pashby, "Deposition of Ti-6Al-4V using a high power diode laser and wire, part I: Investigation on the process characteristics", *Surface & Coatings Technology,* vol. 202, no. 16, pp. 3933-3939, 2008.

[7] E. Brandl, V. Michailov, B. Viehweger and C. Leyens, "Depositiom of Ti-6Al-4V using a laser and wire, part I: Microstructural properties of single beads", *Surface & Coatings Technology,* vol. 206, no. 6, pp. 1120-1129, 2011.

[8] S. Rios, P.A. Colegrove, and S.W. Williams, "Metal transfer modes in plasma wire + arc additive manufacture", *Journal of Materials Processing Technology,* vol. 264, pp. 45-54, 2019.

[9] D.A. Gaponova, R.V. Rodyakina, A.V. Gudenko and A.P. Sliva, "Effect of reheating zones in additive manufacturing by means of electron beam metal wire deposition method", *CIRP Journal of Manufacturing Science and Technology,* vol. 28, pp. 68-75, 2020.

[10] N.I.S. Hussein, J. Segal, D.G. McCartney and I.R Pashby, "Microstructure formation in Waspaloy multilayer builds following direct metal deposition with laser and wire", *Materials Science and Engineering A,* vol. 497, no. 1-2, pp. 260-269, 2008.

[11] R.S. Razavi, "Laser beam welding of Waspaloy: Characterisation and corrosion behavior evaluation", *Optics & Laser Technology,* vol. 82, pp. 113-120, 2016.

[12] J. Lawrence, *Advances in Laser Material Processing*. Coventry: Woodhead Publishing, 2018.

[13] N.I.S. Hussein, M.N. Ayof, M.A. Sulaiman, D.G. McCartney and I.R. Pashby,"Tensile properties, microstructure and microhardness analysis of directly deposited Waspaloy by Gas Tungsten Arc Welding", *Malaysian Journal of Microscopy*, vol. 16, no. 2, pp. 1-10, 2020.

[14] J. Andersson, "Weldability of precipitation hardening of superalloys – influence of microstructure", Ph.D. dissertation, Department of Materials and Manufacturing Technology, Chalmers University of Technology, Goterborg, Sweden, 2011.

[15] X. Chen, Z. Yao, J. Dong, H. Shen and Y. Wang, "The effect of stress on primary MC carbides degeneration of Waspaloy during long term thermal exposure", *Journal of Alloys and Compounds,* vol. 735, pp. 928-937, 2018.

[16] Y. Zhang, L. Yang, W. Lu, D. Wei, T. Meng and S. Gao," Microstructure and elevated temperature mechanical properties of IN718 alloy fabricated by laser metal deposition", *Materials Science & Engineering A,* vol. 771, pp. 1-11, 2020.